Computer Aided Geometric Design 62 (2018) 206–216

Contents lists available at ScienceDirect

Computer Aided Geometric Design

www.elsevier.com/locate/cagd

Accurate geometry modeling of vasculatures using implicit fitting with 2D radial basis functions

Qingqi Hong [a], Qingde Li [b], Beizhan Wang [a], Kunhong Liu [a], Fan Lin [a], Juncong Lin [a], Xuan Cheng [a], Zhihong Zhang [a], Ming Zeng [a,*]

[a] Software School, Xiamen University, Xiamen, China
[b] School of Engineering and Computer Science, University of Hull, UK

ARTICLE INFO

Article history:
Available online 22 March 2018

Keywords:
Geometry modeling
Vasculature
Implicit fitting

ABSTRACT

Accurate vascular geometry modeling is an essential task in computer assisted vascular surgery and therapy. This paper presents a vessel cross-section based implicit vascular modeling technique, which represents a vascular surface as a set of locally fitted implicit surfaces. In the proposed method, a cross-section based technique is employed to extract from each cross-section of the vascular surface a set of points, which are then fitted with an implicit curve represented as 2D radial basis functions. All these implicitly represented cross-section curves are then being considered as 3D cylindrical objects and combined together using a certain partial shape-preserving spline to build a complete vessel branch; different vessel branches are then blended using a extended smooth maximum function to construct the complete vascular tree. Experimental results show that the proposed method can correctly represent the morphology and topology of vascular structures with high level of smoothness. Both qualitative comparison with other methods and quantitative validations to the proposed method have been performed to verify the accuracy and smoothness of the generated vascular geometric models.

1. Introduction

3D visualization of vascular structures is of practical value and importance within the field of computer assisted vascular analysis and morphometry (Preim and Oeltze, 2008). Direct volume rendering (DVR) technique is one of the most popular methods for the 3D visualization of vessels structures contained in a volume dataset. The image generated in this way can be quite suitable for the task of diagnosing vascular disease. However, just to be able to visualize the hidden vascular structures is far from sufficient. The accurate modeling of vascular geometry is essential in many other clinical applications. For vascular intervention planning, it is not an easy task to understand the topology of a vessel tree without the actual vascular geometry. In the case of computer-guided vascular surgery, it can be very difficult to accurately locate the vessel objects directly from the generated image by DVR technique. In addition, the accurate vascular models are of utmost importance to perform reliable simulations of blood flow (computational hemodynamic) (Kretschmer et al., 2013), which enables the study of hemodynamic characteristics such as wall shear stress and intra-aneurysmal flow patterns. A specific vascular geometry model enables us to design and evaluate possible modification of personalized vasculature, which is helpful for the treat-

* Corresponding author.
E-mail addresses: hongqq@gmail.com (Q. Hong), zengming@xmu.edu.cn (M. Zeng).

https://doi.org/10.1016/j.cagd.2018.03.006
0167-8396/

ment decision-making on vascular diseases. Furthermore, the modeling of vascular geometry is also the primary issue that needs to be solved for computer aided vascular surgery, and future fully automatic unmanned vascular surgery. Without the accurate information of vascular geometry, the computer-controlled manipulator is unable to perform the accurate collision detection, and therefore cannot achieve a fine vascular surgery.

In this paper, we propose to model the smooth vascular geometry based on automatic vessel segmentation. Usually, the segmented dataset is represented as a discrete point set, which is prone to produce poor visualization result and not suitable for the tasks required in many clinical applications, such as vessel shape analysis, blood flow simulation, vascular surgery planning and simulation, and so on. In addition, none of current segmentation methods can guarantee a perfect segmentation in all clinical scenarios, thus it is inevitable to perform a manual inspection of the automatically generated segmentation results to meet the requirements of different clinical cases (Kretschmer et al., 2013). In consequence, the accurate geometry modeling of vasculatures from the automatic vessel segmentation is necessary and essential to the clinical applications of vascular surgery and therapy.

Generally, the methods for modeling vascular geometry can be classified into two categories: explicit modeling and implicit modeling. Explicit modeling methods utilise either polygon meshes or parametric functions, e.g. non-uniform rational B-spline (NURBS) function to represent vascular surfaces. Explicit technique is relatively mature, and the explicitly modelled shapes are very efficient for rendering, thus, the explicit technique is widely applied to the geometry modeling of vasculatures in many medical software systems. However, explicitly modelled vasculatures are not suitable for computer assisted surgery, as performing collision detection for explicitly represented surfaces is a very challenging task, which is the primary problem needing to be solved for computer assisted vascular surgery. On the other hand, implicit modeling technique represents a geometric shape as a field function and has received increasing attention recently due to their natural way of representing solid objects and their innate properties on soft shape blending. In addition, when vasculatures are modelled as implicit functions, the problem of collision detection can be easily solved, as it is easy and convenient to tell whether a point lies inside or outside the vascular structures (Bartz, 2005). Implicit modeling techniques are particularly suitable for modeling branching geometric objects as modeling a complex tree-like geometric object can be reduced to a problem of modeling a set of cylindrical geometric objects, which is a very simple geometric modeling task. Hence, implicit modeling technique has great advantages over explicit method in future computer assisted automatic surgery.

In this paper, a new method is developed for the accurate geometry modeling of vasculatures based on the vascular centreline descriptions. In the proposed method, a set of points depicting the profiles of the vessel's cross-sections is extracted first using a cross-section based vascular-specific method. The extracted point set is then fitted with an implicit curve represented as 2D radial basis functions (Li et al., 2004). Then all the implicitly represented cross-sections are blended flexibly along the centreline using the partial shape-preserving splines (Li and Tian, 2011) to build smooth vessel branches; finally, different vessel branches are blended using the extended smooth maximum function (Li, 2007) to construct the complete vascular tree. The presented experiment results show that the modelled vascular shapes are of high smoothness and faithfulness. In addition, some qualitative and quantitative comparison with other methods have been carried out for the proposed technique to validate the accuracy and smoothness of the generated vascular models.

2. Related work

2.1. Vascular modeling

In general, the techniques for modeling vascular geometry can be classified into two groups: explicit modeling method and implicit modeling method. In explicit modeling methods, a vascular surface is represented as polygon meshes or parametric functions. As the explicitly modelled shapes are very efficient for rendering, various explicit modeling methods have been proposed for the geometry modeling of vasculatures in the last two decades. A representative instance is to utilize simple cylinder-like geometric primitives, such as cylinders (Masutani et al., 1996) or truncated cones (Hahn et al., 2001), to construct the vascular surfaces. In order to achieve smooth transition at the points of branching, several advanced explicit modeling techniques have been suggested to construct vascular shapes along the centreline (Höhne et al., 2000; Felkel et al., 2004; Bornik et al., 2005; Wu et al., 2011; Wang et al., 2016). However, it is generally not an easy task to perform shape blending operations and ramifications for explicit methods (Bloomenthal, 1995).

On the other hand, implicit modeling techniques developed in Bloomenthal's work (Bloomenthal, 1995) can be applied to reconstruct the geometry of vascular structures. Implicitly represented geometric objects are inherently easy to combine in various ways, which make it simple to implement ramification. However, there is still a long way to go for existing implicit modeling techniques to achieve a satisfactory result that meets the requirements of accurate computer-aided diagnosis and treatment of vascular diseases. The implicit vascular geometry modelled using convolution surfaces (CS) (Oeltze and Preim, 2005) is only a morphological approximation, and the quality of the resulting surfaces based on multi-level partition of unity implicits (MPUIs) (Schumann et al., 2007; Schumann et al., 2008) is generally poor and has to be improved using an additional remeshing step. The developed modeling techniques of vascular geometry (Hong et al., 2012; Hong, 2013; Hong et al., 2016) based on piecewise algebraic splines (PAS) (Li and Tian, 2009) can reconstruct vascular tree with excellent quality. However, the accuracy of the reconstructed vasculatures will be greatly affected in the case of highly curved centreline. Kretschmer et al. (2013) presented a vascular modeling method based on sweep surfaces, which can generate and correct smooth high-quality vascular structures. However, this method can only guaranteed C^1 continuity of the model

surface. Recently, Kerrien et al. (2017) presented a local implicit modeling (LIM) algorithm to improve the methods proposed by Tsingos et al. (1995) and Bittar et al. (1995), with a more efficient energy formulation and a more discriminative blob selection criterion. The LIM method is claimed to fully automatically and accurately fit surfaces to data points, despite holes and noise.

2.2. Implicit surface modeling using radial basis functions

One of the most popular techniques for implicit surface modeling is to use blobby objects. In this technique, an object is implicitly represented as a collection of blobs, each of which could be considered as a point energy with an influence field that decreases with the increase of distance from the source of energy (Li et al., 2004). In general, the potential field of influence can be defined as a function of distance r, such as $\Phi(r) = e^{-ar^2}$, which is a commonly used type of radial basis function. For simplicity and computational efficiency, radial basis functions are also often defined as increasing functions of distance r, especially when radial basis functions are used together with polynomial functions, such as those used in polyharmonic splines. With radial basis functions, we can define an implicit surface as a level set of the weighted sum of a collection of metaballs with their centres at $\{P_i\}_{i=1}^n$ respectively: $\sum_{i=1}^{n} \lambda_i \Phi_i(r)$ (Ricci, 1973), where $\Phi_i(r)$ corresponds to the metaball with centre $\mathbf{P}_i$. Radial basis functions have several advantages when applied to data fitting in geometric modeling, such as the adjustable local influence as well as the invariance under Euclidean transformation. Hence, increasing attentions have been given on the research of reconstructing implicit surfaces from scattered points using radial basis functions (Li et al., 2004; Carr et al., 1997; Carr and Beatson, 2001; Turk and O'Brien, 2002). In these techniques, an implicit surface can be represented by the candidate functions in the following form:

$$F(\mathbf{P}) = \sum_{i=1}^{n} \lambda_i \Phi_i(\|\mathbf{P} - \mathbf{P}_i\|) + \rho(\mathbf{P}) \tag{1}$$

where $\mathbf{P} = (x, y, z)$ is an arbitrary point in 3D space $\mathbf{R}^3$, and $\rho(\mathbf{P})$ is a low degree polynomial, which can be chosen as a constant, linear, or quadratic. Generally, the degree of polynomial $\rho(\mathbf{P})$ should not be chosen larger than four, as it becomes increasingly difficult to control the fitting results with the increasing degree of the polynomial (Keren et al., 1994). Inspired by Fitzgibbon et al.'s work (1999), Li et al. (2004) developed an implicit fitting algorithm based on radial basis functions with ellipsoid constraint, in which the polynomial part $\rho(\mathbf{P})$ is always constrained to an ellipsoid expression. Compared with other implicit fitting techniques, the technique based on radial basis functions with ellipsoid constraint does not need to use information on surface normal but still can fit the data accurately. One appealing feature of radial basis functions with ellipsoid constraint is that even the data to be fitted is quite sparse, incomplete or even with big holes, a relatively meaningful fitting can still be achieved with radial basis functions with ellipsoid constraint. The algorithm is straightforward to implement, as it is a one-step fitting based on solving a simple general eigen-system (Li et al., 2004). As our method is cross-section based, what we used in this research is actually the 2D version of radial basis functions with ellipsoid constraint, where the constraint term $\rho(\mathbf{P})$ becomes an ellipse.

3. Proposed method

There are three main steps in our proposed vessel modeling method. Firstly, each set of control points for each vessel cross-section obtained from a vascular segmentation process is fitted using 2D radial basis functions based on the local Frenet frame; then, by performing a distance mapping along the vessel centreline, all the implicitly represented cross-section contours are blended flexibly using the partial shape-preserving splines to build vessel branches; finally, different vessel branches are blended using the extended smooth maximum function to construct the complete vascular tree.

3.1. Accurate implicit curve fitting of vessel cross-section profile with 2D radial basis functions

3.1.1. The extraction of control points for the specification of vessel cross-sections

Suppose $\mathbf{S}(s)$ is the parametric curve that represents the centreline of a vessel branch, and $\mathbf{S}(s_i)$ is a knot point on the centreline; then, we can extract the control points for specifying the cross-section based on $\mathbf{S}(s_i)$ in the following steps:

(1) Calculate the Frenet frame based on $\mathbf{S}(s_i)$. Frenet frame can be intuitively constructed by calculating the tangent $\mathbf{T}$, normal $\mathbf{N}$, and binormal $\mathbf{B}$ vectors. The calculation of $\mathbf{T}$, $\mathbf{N}$, $\mathbf{B}$ based on the centreline point $\mathbf{S}(s_i)$ are given by:

$$\begin{aligned} \mathbf{T}(s_i) &= \frac{\mathbf{S}(s)'}{\|\mathbf{S}(s)'\|}\,|_{s=s_i} \\ \mathbf{N}(s_i) &= \frac{\mathbf{S}(s)''}{\|\mathbf{S}(s)''\|}\,|_{s=s_i} \\ \mathbf{B}(s_i) &= \mathbf{T}(s_i) \times \mathbf{N}(s_i) \end{aligned} \tag{2}$$

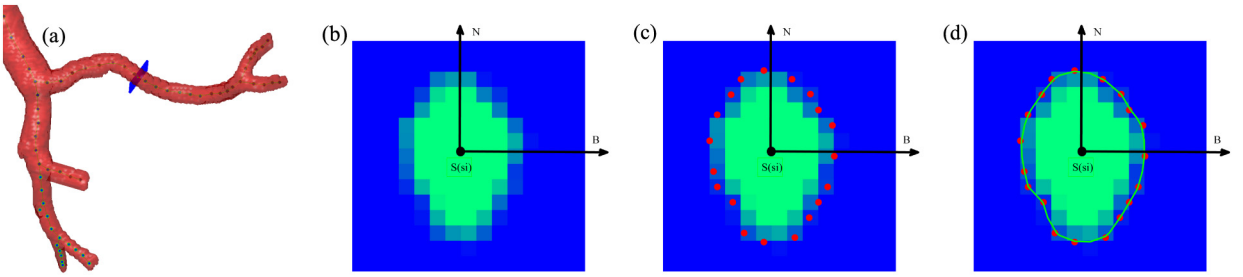

Fig. 1. The specification of vessel cross-section with 2D radial basis functions. (a) Moving the defined rectangle to intersect with the vessel surface. (b) Mapping the intensive value of the segmented vessel image into the rectangle. (c) The extraction of contour points with zero intensive value. (d) The smooth implicit curve specified by the extracted contour points using 2D radial basis functions with ellipse constraint. (For interpretation of the colours in the figure(s), the reader is referred to the web version of this article.)

(2) For each knot position $\mathbf{S}(s_i)$, specify a rectangle based on the Frenet-frame defined at $\mathbf{S}(s_i)$ such that it is normal to $\mathbf{T}$ and its edges are aligned with the Binormal unit vector $\mathbf{B}$ and Normal unit vector $\mathbf{N}$ (see Fig. 1(a)).

(3) Map the intensity of the segmented vascular image into the defined rectangle, and extract the contour points with zero intensive value. Since the shape of vessel can be identified as the voxels with intensive value ≥ 0 after the process of segmentation, we can conveniently extract the voxel points with zero intensive value as the control points for specifying the vessel cross-sections. As shown in Fig. 1(b), the region inside the vessel is denoted as the green pixels (intensive value lager than zero); while the region outside the vessel is denoted as the blue pixels (intensive value smaller than zero). Fig. 1(c) shows the extracted contour points with zero intensive value (denoted as the red points).

3.1.2. Accurate cross-section fitting with 2D radial basis functions

Let $\{\mathbf{P}_i^{\dagger}\}(b,n)(i=1,2,\ldots,N)$ be a set of contour points extracted from the cross-section of vessel surface regarding the bn-coordinate plane of the Frenet frame. In the Frenet frame space, $\mathbf{P}_i^{\dagger}$ is considered as 2D data point, and then the fitting technique presented in section 2.2 becomes an implicit curve fitting. Let $\triangle$ be the 2D control polygon defined by the set of points, the corresponding implicitly fitted curve representing the vessel cross-section contour can be specified by the formula:

$$C_{\triangle}(\mathbf{P}^{\dagger}) = \sum_{i=1}^{n} \lambda_i \Phi_i(\left\| \mathbf{P}^{\dagger} - \mathbf{P}_i^{\dagger} \right\|) + \rho(\mathbf{P}^{\dagger}) = 0 \tag{3}$$

In which $\mathbf{P}^{\dagger}$ is the arbitrary 2D data point in the Frenet frame plane. As this is a 2D curve fitting, the constrained polynomial part in the fitting model now corresponds to an ellipse. Thus, the polynomial part in formula 3 is replaced by Li et al. (2004):

$$\rho(\mathbf{P}^{\dagger}) = Ab^2 + 2Bbn + Cn^2 + 2Eb + 2Fn + G \tag{4}$$

where the constraint for the polynomial is $AC - B^2 > 0$.

Fig. 1(d) demonstrates the vessel cross-section contour is accurately specified by the curve fitting with $C_{\triangle}(\mathbf{P}^{\dagger}) = 0$ using radial basis functions with ellipse constraint, which is the interpolating implicit curve and can go through all the control points.

3.2. Combining implicit cross-section profiles using shape-preserving implicit splines

3.2.1. Extruding 2D cross-section profile along the centreline

Once the freeform cross-section is specified in its local Frenet frame, we can conveniently extrude the 2D implicit curve along the centreline $\mathbf{S}$ by means of distance mapping to generate a 3D implicit surface. Suppose $\mathbf{P}(x,y,z)$ is an arbitrary point in 3D space $\mathbf{R}^3$, and the distance mapping is performed by the following steps:

(1) Calculate the centreline point $\mathbf{S}(s_0)$ that is closest point to $\mathbf{P}$; that is, s_0 satisfies

$$\| \mathbf{P} - \mathbf{S}(s_0) \| = \mathbf{min}_s(\| \mathbf{P} - \mathbf{S}(s) \|) \tag{5}$$

(2) Transform $\mathbf{P}(x,y,z)$ to the tangent space point $\mathbf{P}^{\dagger}(b,n,t)$ based on the corresponding Frenet-frame of $\mathbf{S}(s_0)$:

$$\begin{aligned} b &= \overrightarrow{\mathbf{P} - \mathbf{S}(s_0)} \cdot \mathbf{B}(s_0) \\ n &= \overrightarrow{\mathbf{P} - \mathbf{S}(s_0)} \cdot \mathbf{N}(s_0) \\ t &= s_0 \end{aligned} \tag{6}$$

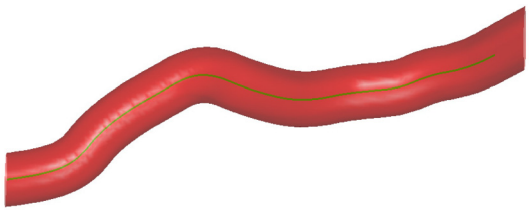

Fig. 2. An extruded implicit surface model along arbitrary centreline from the cross-section profiles specified in Fig. 1(d).

in which $\cdot$ is the scalar product of two vectors; $\mathbf{B}(s_0)$ is the binormal unit vector on the Frenet-frame of $\mathbf{S}(s_0)$; and $\mathbf{N}(s_0)$ is the normal unit vector on the Frenet-frame of $\mathbf{S}(s_0)$.

Suppose the cross-section profile is represented as $C_{\triangle}(\mathbf{P}^{\dagger}(b,n,t))=0$ in its local Frenet frame, then by performing the distance mapping: $b=X(x,y,z)$, $n=Y(x,y,z)$ and $t=Z(x,y,z)$, the extruded implicit surface can be represented as:

$$F(x,y,z)=C_{\triangle}(\mathbf{P}^{\dagger}(X,Y,Z))=0 \tag{7}$$

which constructs an implicit tubular shape along its centreline from the specified cross-section. Fig. 2 shows an extruded implicit surface model along arbitrary centreline from the cross-section profiles specified in Fig. 1(d).

3.2.2. Modeling of the freeform implicit surface along the centreline with varying cross-sections

Unlike 3D parametric spline surfaces, 3D implicit surfaces can be described as the result of blending a set of 2D implicit control curves using spline basis functions. One simple way is to design a freeform implicit surface as a weighted sum of a set of 2D contour curves distributed along a coordinate axis (i.e. z-axis), as the method presented in Li and Tian (2009). In order to model the freeform implicit surfaces along a given curved centreline, not limited to straight coordinate axis, we can perform a distance mapping, and define an overall implicit surface as the weighted sum of the sequence of cross-section profiles distributed along the given centreline. The required implicit surface model can be described implicitly in the Frenet-frame space by the following formula:

$$f(b,n,t)=\sum_{j=1}^{L} C_{\triangle,j}(\mathbf{P}^{\dagger}(b,n,t))B_j(t-s_j)=0 \tag{8}$$

in which $C_{\triangle,j}(\mathbf{P}^{\dagger}(b,n,t))$ is the implicitly defined cross-section based on the j-th centreline point; and $B_j(t-s_j)$ is the shape-preserving implicit spline function (Li and Tian, 2011) based on the j-th centreline point; b, n and t respectively are defined in the Frenet-frame space according to Equations (6); $\{s_j\}$ is a list of knots for the parametric position of centreline $\mathbf{S}(s)$; L is the number of cross-sections. We choose the sample centreline points in an interval d for defining cross-section, as it is unnecessary to define the cross-section for every centreline point. And $B_j(t-s_j)$ in Equation (8) is expanded as following:

$$B_j(t-s_j)=B^m_{[-d/2,d/2],\delta}(t-s_j) \tag{9}$$

In which the general spline basis function $B^m_{[a,b],\delta}(x)$ is defined as Li and Tian (2009):

$$B^{(m)}_{[a,b],\delta}(x)=H_m(\frac{b-x}{\delta})-H_m(\frac{a-x}{\delta}) \tag{10}$$

where $[a,b]$ is an interval with $a\le b$; $H_m(x)$ is the smooth unit step function introduced in Li et al. (2006); and δ is the smooth parameter for controlling the blending range. For a given centreline $\mathbf{S}$, by performing the mapping presented in Subsection 3.2.1: $b=X(x,y,z)$, $n=Y(x,y,z)$ and $t=Z(x,y,z)$, the implicit surface model described in the Frenet-frame space can be transformed to $\mathbf{R}^3$ space by the following form:

$$\begin{aligned} F(x,y,z)&=f(b,n,t)\\ &=f(X(x,y,z),Y(x,y,z),Z(x,y,z))=0 \end{aligned} \tag{11}$$

As presented in Fig. 3, a vessel branch is modelled as a weighted sum of the nine variable cross-sections along the centreline with the shape-preserving implicit spline functions. (a) shows the nine defined rectangles intersecting with a vessel branch, and (b) presents the corresponding cross-section contours specified by the fitting curves with 2D radial basis functions. (c) is the vessel branch model constructed as a weighted sum of the nine variable cross-sections along the centreline.

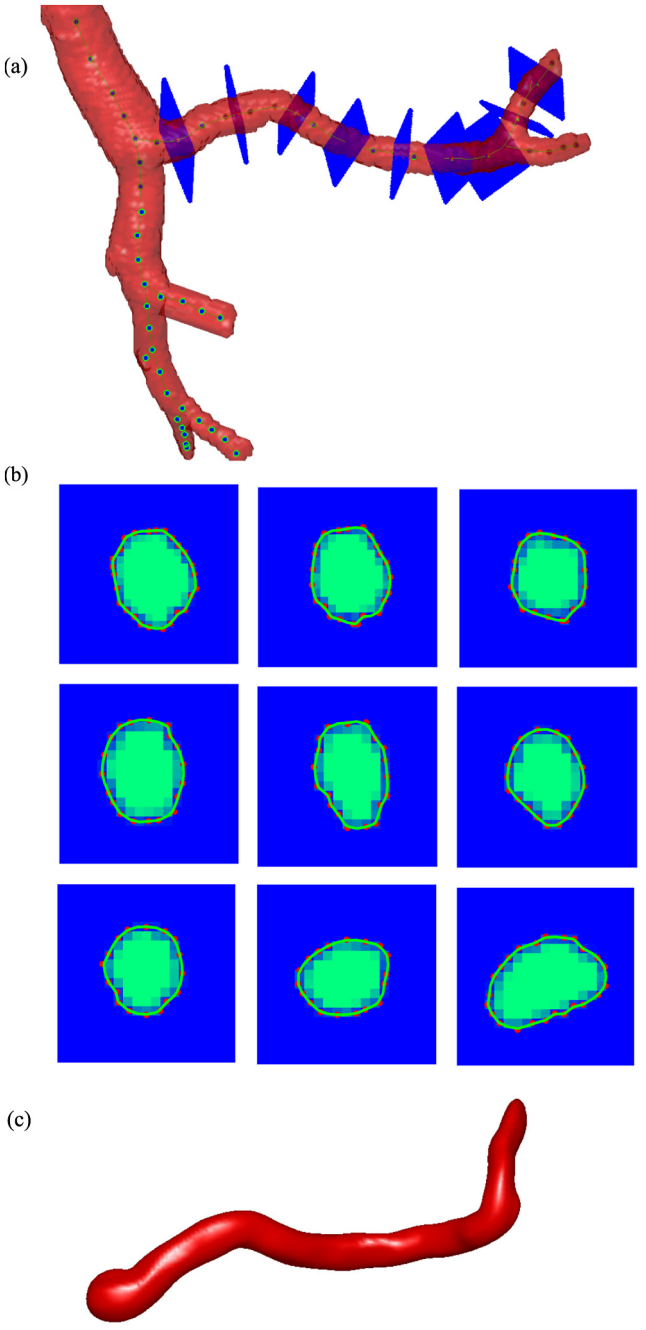

Fig. 3. The modeling of a vessel branch by weighted summing nine variable cross-sections along the centreline with the shape-preserving implicit spline functions. (a) The nine defined rectangles intersecting with a vessel branch. (b) The corresponding cross-section contours specified with 2D radial basis functions. (c) The vessel branch model constructed as a weighted sum of the nine variable cross-sections.

3.3. Combining vessel branches using the extended smooth maximum function

The implicitly defined shapes of different branches need to be carefully blended to construct the overall implicit surfaces corresponding to the entire tree structure. In order to achieve a smooth shape-preserving blending, we employ the extended smooth maximum function to blend different implicitly-defined objects together. The extended smooth maximum function is defined in Li (2007):

$$max_{n,\delta}(x, y) = \frac{1}{2}(x + y + |x - y|_{n,\delta}) \tag{12}$$

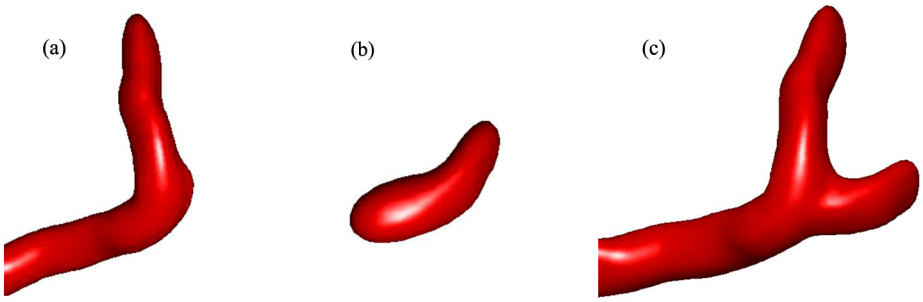

Fig. 4. Smooth and accurate blending of two implicitly defined vessel branching models with the smooth maximum function. (a) and (b) represent two individual vessel branching models, and (c) represents the blending result of these two models by using the extended smooth maximum function.

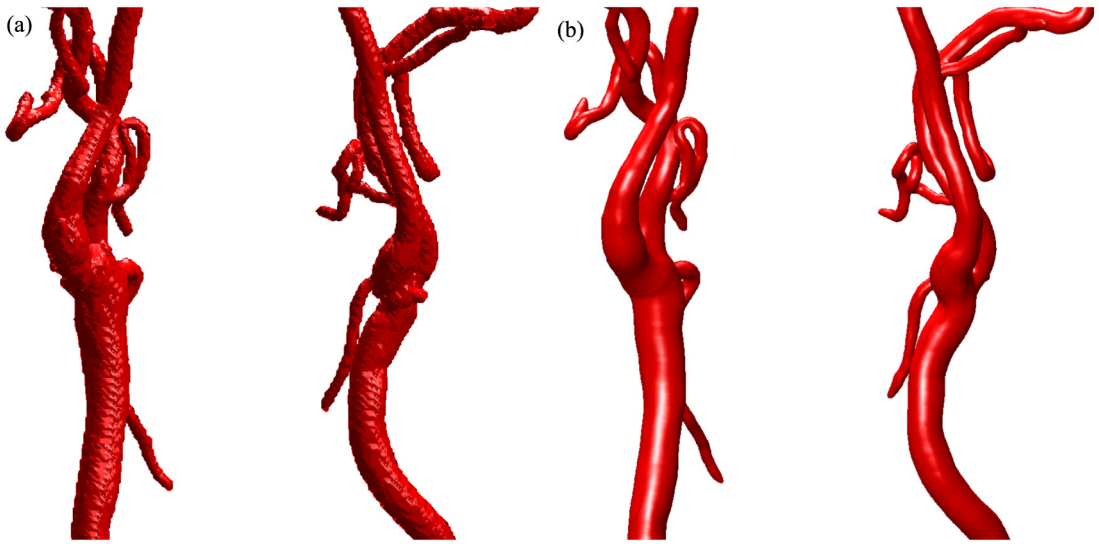

Fig. 5. The modeling of CTA Carotid Artery. (a) The isosurface rendering of segmentation result. (b) The modeling result using our method.

where $|x|_{n,\delta}$ is a kind of smooth absolute function with degree of smoothness n and blending range-control parameter δ. Suppose F_1 and F_2 are two implicit shapes constructed from different centrelines, the smooth blending of these two implicit shapes can be achieved by the following operation:

$$F_{blend} = max_{n,\delta}(F_1, F_2) = \frac{1}{2}(F_1 + F_2 + |F_1 - F_2|_{n,\delta}) \tag{13}$$

As shown in Fig. 4, two implicitly defined vessel branching models are smoothly and accurately blended, where the two original vessel shapes are kept unchanged except the regions close to their joint. (a) and (b) represent two individual vessel branching models, and (c) represents the blending result of these two models by using the extended smooth maximum function $max_{n,\delta}(x, y)$.

4. Results and discussion

4.1. Modeling results based our method

We have applied the proposed method to several 3D medical datasets for the geometry modeling of vasculatures. Two typical modeling results are shown in Fig. 5 and 6, representing the representative vascular structures in the human body. One example is the modeling of Carotid Artery from the 3D magnetic resonance angiography (MRA) images with a resolution of $512 \times 512 \times 206$. Fig. 5(a) is the isosurface rendering of segmentation result of carotid artery, and (b) is the corresponding modeling result with our method. The other example is the modeling of Liver Portal Vein from the 3D computerized tomography angiography (CTA) images with a resolution of $512 \times 512 \times 300$. Similarly, Fig. 6(a) is the isosurface rendering of segmented liver portal vein, and (b) is the corresponding modeling result with our method. As presented in the figures, the isosurface rendering of segmentation results suffers from aliasing artifacts and diverges considerably from the real vessels. On the other hand, our modeling method can generate vascular models with superior visual quality and produce smooth transitions at branchings. From the visual comparison between our modeling results and the segmentation results,

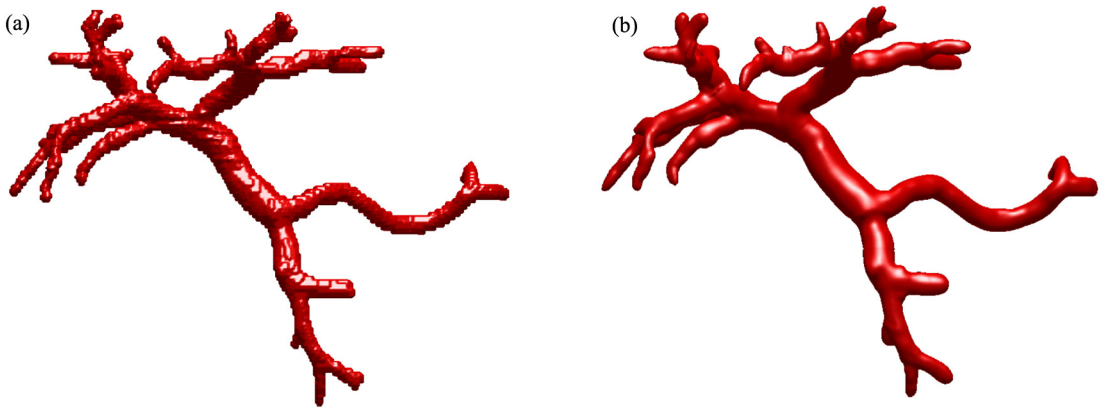

Fig. 6. The modeling of segmented liver portal vein. (a) The isosurface rendering of segmentation result. (b) The modeling result using our method.

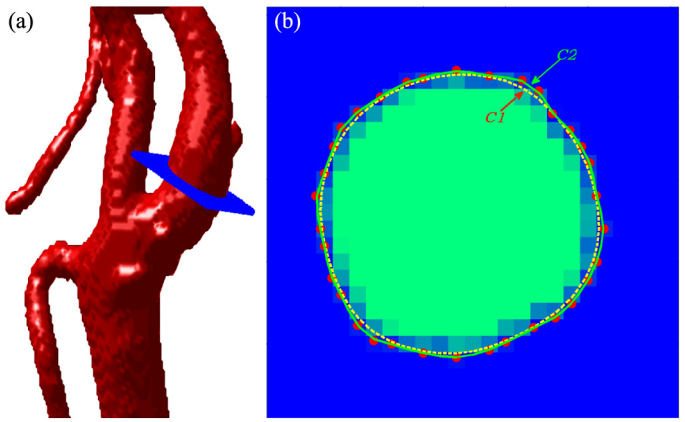

Fig. 7. The comparison between PAS method and our method for the specification of vessel cross-section contour. (a) The defined rectangle intersecting with a vessel branch; (b) the specification of cross-section contour by PAS method and our method.

we can conclude the preliminary judgment that the morphology and topology of vascular structures, even very thin and curved branches, can be correctly and faithfully modelled using the proposed method.

4.2. Comparison with the method based on PAS

In this section, we investigation the qualitative comparison between our proposed method and the technique based on PAS, since it is also a centreline based implicit modeling method and can achieve vascular models with superior quality. Generally, the proposed method has two main differences with the PAS based technique. Firstly, our method uses the implicit fitting technique with 2D radial basis functions to specify the vessel cross-section contours instead of 2D PAS. The implicit fitting technique with 2D radial basis functions can construct interpolating implicit curves (see the solid green curve C_2 in Fig. 7(b)), which is able to go through all the control points; while the 2D PAS is a kind of approximating implicit curve, which is unable to go through all the control points (see the dashed yellow curve C_1 in Fig. 7(b)). That is, the implicit fitting technique with 2D radial basis functions can specify the vessel cross-section more accurately than 2D PAS technique does.

The other difference is the distance mapping way for extruding the implicit surface along the centreline. In PAS based technique, the orthonormal basis was firstly defined by the local Frenet frame at each sampled skeletal point, and then the coordinates of the relative point were transformed into its local Frenet frame space. In this distance mapping way, implicit surface is extruded along several straight-line segments to simulate the curved centreline. In the case of much curved centreline, if distance between the neighbour skeletal points is not small enough, the extruded implicit surface will suffer from strong discontinuity (see Fig. 8(b)). On the other hand, in radial basis functions with ellipse constraint based technique, we firstly find out the nearest skeletal point for the arbitrary point in 3D space, and then transform this 3D point's coordinate into the local Frenet frame space defined at its nearest skeletal point. The distance mapping way actually remapping the 3D point's coordinate into the distance field along the centreline, which enables to extrude the implicit surface along any given curved centreline. As shown in Fig. 8(c), our method can achieve the same excellent smoothness as the PAS based technique.

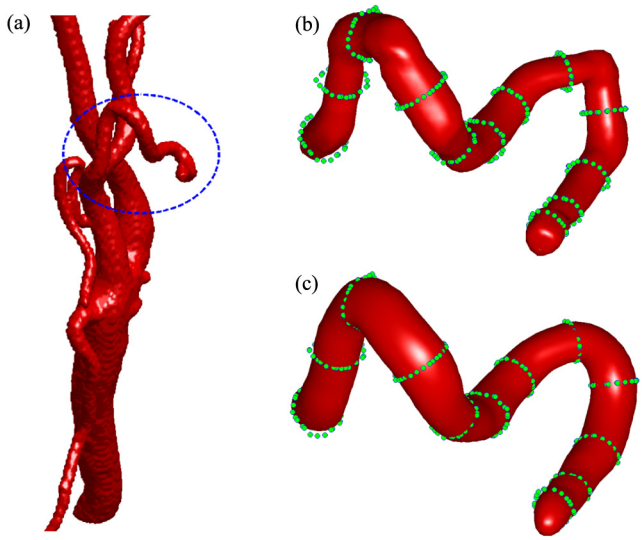

Fig. 8. The comparison between PAS method and our method for extruding implicit surface models along a very curved centreline. (a) The overview of the segmented vessel tree and the very curved branch for modeling indicated the ellipse. (b) The modeling result of the curved branch based on PAS method. (c) The modeling result of the curved branch based on our method.

Table 1
Quantitative comparison between our proposed method and the MPUI based method and the PAS based method for the modeling of different vascular datasets. Distance values are related to *voxDiag*. The accuracy is measured by calculating the mean distance between the segmentation results and the generated models, and the smoothness is estimated by measuring the AUMC of the reconstructed surface.

Data sets	MPUI based method		PAS based method		The proposed method	
	Distance	AUMC	Distance	AUMC	Distance	AUMC
Carotid Artery	0.51	0.26	0.33	0.21	0.26	0.26
Liver Portal Vein	0.47	0.19	0.36	0.12	0.33	0.16
Cerebral Vasculatures	0.35	0.54	0.33	0.28	0.28	0.25

4.3. Validation

Besides the visual inspection, it is necessary to perform the quantitative validation analysis for estimating whether the underlying data are faithfully represented with certain smoothness (Preim and Oeltze, 2008). We calculate the mean Euclidean distance between the segmented data and the generated model for judging the modeling accuracy. We describe the deviation in relation to the resolution of the test dataset, i.e. length of the voxel diagonal (voxDiag) (Schumann et al., 2008). For estimating the smoothness, we calculate the average of the unsigned mean curvatures (AUMC) for all voxels on the modelled surface, which is a effective indicator for examining the degree of smoothness of the surface (Dong and Wang, 2005).

Table 1 shows the direct quantitative comparisons between our proposed method and the MPUI based Method and the PAS based method for the modeling of different vascular datasets. The smaller Distance values represent the more accurate generated model, and the smaller AUMC values represent the smoother generated model. As showed in the table, the mean deviations corresponding to the models built from our method are much smaller than that based on the MPUI method and PAS method for each experimental data set. In other words, our method can achieve more accurate vessel models than the other two methods. Although the AUMCs of our built models are not the smallest, they are very close to that based on PAS method, which is regarded as an excellent approach to model vessel tree with great smoothness property (Kretschmer et al., 2013). For the Carotid Artery dataset, the AUMC based on our method is even smaller than that based on PAS method. The validation results demonstrate that the proposed modeling method is able to generate highly accurate vascular models with certain smoothness.

4.4. Computational complexity

Generally, the time complexity of the proposed method depends on the complexity of the vascular tree as well as the resolution of input dataset. In addition, the interval d in Equation (9) for defining cross-section will also affect the efficiency of the proposed method. In general, the value of interval d is set to be proportional to radius of the current defined cross-section, which can guarantee a reasonable trade-off between efficiency and accuracy. To demonstrate the

Table 2
Performance measurements of the proposed method for the geometry modeling of anatomic vasculares carried out on an Intel Core i5 CPU with two cores @1.6GHz and 8GB RAM. The computational time is measured in seconds.

Datasets	Resolution	Number of vertices	Number of faces	Time (second)
Carotid Artery	$512 \times 512 \times 206$	67933	135745	20.12
Liver Portal Vein	$512 \times 512 \times 300$	65918	131788	82.26
Cerebral Vasculatures	$352 \times 442 \times 114$	63870	137324	35.70

computational cost of our algorithm, Table 2 presents the information concerning the complexity of the resulting models and the computational time of the proposed based on the medical datasets used above.

5. Conclusion

This paper presents a novel method for the accurate geometry modeling of vasculatures based on geometric centreline descriptions. Generally, the proposed method has two ingredients to achieve accurate vascular models. Firstly, compared to other methods based on regular spline interpolation, the proposed method is an implicit modeling technique, which is easy to perform blending for different geometric objects in various ways and has the intrinsic attribute of representing volumetric objects. In addition, the proposed technique is based on 2D radial basis functions with ellipse constraint, which can accurately specify the vessel cross-section profiles even with sparse control points. The other ingredient is the distance mapping method for extruding the implicit surface along the centreline. In the proposed method, we remap the 3D points into the distance field along the centreline, which enables to extrude the implicit surface continuously along highly curved centreline and achieve cylindrical model with excellent smoothness. The proposed distance mapping method can be extended to construct generalized cylinders along any given curved centreline with high-smoothness quality. Qualitative validations have illustrated that the proposed technique can construct more precise vascular models than the MPUI based method and the PAS based method.

The proposed method is based on the extracted centreline of the vascular tree. However, the centreline extraction of vasculatures is not an easy task, and may involve certain manual interventions. One of our future work is to develop more automatic and robust method for extracting the centreline of vascular structures. The design and evaluation of the possible modification of personalized vascular model is helpful to choose the optimal interventional procedures for treating vascular diseases. Another area of our future work is on developing implicit geometry-editing technique to support direct interactive modification of patient-specific vascular models, and to conduct the computational simulation of the blood flow within the constructed and modified vascular models to demonstrate effectiveness of planned treatments of the diseased vascular structure.

Acknowledgements

The authors would like to thank all the anonymous reviewers for their constructive comments. This work is supported by the National Natural Science Foundation of China (Grant No. 61502402, 61772023, and 61402387), the Natural Science Foundation of Fujian Province of China (Grant No. 2015J05129 and 2016J01320), the National Key Technology Research and Development Program of the Ministry of Science and Technology of China (2015BAH55F05), and the Fundamental Research Funds for the Central Universities (Grant No. 20720180073).

References

Bartz, D., 2005. Virtual endoscopy in research and clinical practice. Comput. Graph. Forum 24 (1), 111–126.
Bittar, E., Tsingos, N., Gascuel, M., 1995. Automatic reconstruction of unstructured 3d data: combining a medial axis and implicit surfaces. Comput. Graph. Forum 14 (3), 457–468.
Bloomenthal, J., 1995. Skeletal Design of Natural Forms. Phd thesis. The University of Calgary.
Bornik, A., Reitinger, B., Beichel, R., 2005. Reconstruction and representation of tubular structures using simplex meshes. In: Proceedings of Winter School of Computer Graphics (WSCG), pp. 61–65.
Carr, J., Beatson, R., 2001. Reconstruction and representation of 3d objects with radial basis functions. In: Proceedings of ACM SIGGRAPH 2001, pp. 12–17.
Carr, J.C., Fright, W.R., Beatson, R.K., 1997. Surface interpolation with radial basis functions for medical imaging. IEEE Trans. Med. Imaging 16 (1), 96–107.
Dong, C., Wang, G., 2005. Curvatures estimation on triangular mesh. J. Zhejiang Univ. Sci. A 6, 128–136.
Felkel, P., Wegenkittl, R., Bühler, K., 2004. Surface models of tube trees. In: Proceedings of Computer Graphics International, pp. 70–77.
Fitzgibbon, A., Pilu, M., Fisher, R.B., 1999. Direct least square fitting of ellipses. IEEE Trans. Pattern Anal. Mach. Intell. 21 (5), 476–480.
Hahn, H., Preim, B., Selle, D., Peitgen, H., 2001. Visualization and interaction techniques for the exploration of vascular structures. In: Proceedings of IEEE Visualization 2001 (VIS'01), pp. 395–402.
Höhne, K., Pflesser, B., Pommert, A., 2000. A realistic model of the inner organs from the visible human data. In: Proceedings of Medical Image Computing and Computer-Assisted Intervention. Springer, pp. 776–785.
Hong, Q., 2013. A skeleton-based technique for modelling implicit surfaces. In: Proceedings of the 6th International Congress on of Image and Signal Processing (CISP), pp. 686–691.
Hong, Q., Li, Q., Tian, J., 2012. Implicit reconstruction of vasculatures using bivariate piecewise algebraic splines. IEEE Trans. Med. Imaging 31 (3), 543–553.
Hong, Q., Li, Y., Li, Q., Wang, B., Yao, J., Wu, Q., She, Y., 2016. An implicit skeleton-based method for the geometry reconstruction of vasculatures. Vis. Comput. 32 (10), 1251–1262.

Keren, D., Cooper, D., Subrahmonia, J., 1994. Describing complicated objects by implicit polynomials. IEEE Trans. Pattern Anal. Mach. Intell. 16, 38–53.
Kerrien, E., Yureidini, A., Dequidt, J., Duriez, C., Anxionnat, R., Cotin, S., 2017. Blood vessel modeling for interactive simulation of interventional neuroradiology procedures. Med. Image Anal. 35, 685–698.
Kretschmer, J., Godenschwager, C., Preim, B., Stamminger, M., 2013. Interactive patient-specific vascular modeling with sweep surfaces. IEEE Trans. Vis. Comput. Graph. 19 (12), 2828–2837.
Li, Q., 2007. Smooth piecewise polynomial blending operations for implicit shapes. Comput. Graph. Forum 26 (2), 157–171.
Li, Q., Griffiths, J.G., Ward, J., 2006. Constructive implicit fitting. Comput. Aided Geom. Des. 23 (1), 17–44.
Li, Q., Tian, J., 2009. 2d piecewise algebraic splines for implicit modeling. ACM Trans. Graph. 28 (2).
Li, Q., Tian, J., 2011. Partial shape-preserving splines. Comput. Aided Des. 43, 394–409.
Li, Q., Wills, D., Phillips, R., Viant, W., Griffiths, J., Ward, J., 2004. Implicit fitting using radial basis functions with ellipsoid constraint. Comput. Graph. Forum 23 (1), 55–69.
Masutani, Y., Masamune, K., Dohi, T., 1996. Region-growing-based feature extraction algorithm for tree-like objects. In: Proceedings of Visualization in Biomedical Computing, vol. 1131. Springer, pp. 161–171.
Oeltze, S., Preim, B., 2005. Visualization of vascular structures with convolution surfaces: method, validation and evaluation. IEEE Trans. Med. Imaging 25 (3), 540–549.
Preim, B., Oeltze, S., 2008. 3d visualization of vasculature: an overview. In: Visualization in Medicine and Life Sciences. Springer, pp. 39–59.
Ricci, A., 1973. A constructive geometry for computer graphics. Comput. J. 16 (2), 157–160.
Schumann, C., Neugebauer, M., Bade, R., Peitgen, H.-O., Preim, B., 2008. Implicit vessel surface reconstruction for visualization and cfd simulation. Int. J. Comput. Assisted Radiol. Surg. 2 (5), 275–286.
Schumann, C., Oeltze, S., Bade, R., Preim, B., Peitgen, H.-O., 2007. Model-free surface visualization of vascular trees. In: IEEE/Eurographics Symposium on Visualization, pp. 283–290.
Tsingos, N., Bittar, E., Gascuel, M.-P., 1995. Implicit surfaces for semi-automatic medical organ reconstruction. In: Computer Graphics International'95, pp. 3–15.
Turk, G., O'Brien, J., 2002. Modelling with implicit surfaces that interpolate. ACM Trans. Graph. 21 (4), 855–873.
Wang, X., Wu, Z., Shen, J., Zhang, T., Mou, X., Zhou, M., 2016. Repairing the cerebral vascular through blending ball b-spline curves with g^2 continuity. Neurocomputing 173, 768–777.
Wu, X., Luboz, V., Krissian, K., Cotin, S., Dawson, S., 2011. Segmentation and reconstruction of vascular structures for 3d real-time simulation. Med. Image Anal. 15 (1), 22–34.